3. L. Olesen *et al.*, *ibid.* **72**, 2251 (1994); J. M. Krans and J. M. van Ruitenbeek, *Phys. Rev.* **50**, 17659 (1994); J. M. Krans *et al.*, *Nature* **375**, 767 (1995), and references therein.
4. C. Joachim, J. K. Gimzewski, R. R. Schlittler, C. Chavy, *Phys. Rev. Lett.* **74**, 2102 (1995).
5. N. D. Lang, *Phys. Rev. B* **52**, 5335 (1995).
6. D. M. Eigler, P. S. Weiss, E. K. Schweizer, N. D. Lang, *Phys. Rev. Lett.* **66**, 1189 (1991).
7. D. M. Eigler and E. K. Schweizer, *Nature* **344**, 524 (1990).
8. D. M. Eigler, C. P. Lutz, W. E. Rudge, *ibid.* **352**, 600 (1991).
9. D. M. Eigler and C. P. Lutz, unpublished results.
10. We measured *I* versus *V* and *dI/dV* versus *V*; both measurements indicated that, to within 5%, there was no *V* dependence over the range ±30 mV to the resistances we report here.
11. We have held the voltage drop across the STM junction constant as we extended the *z*-piezo toward the surface. Adjustments in the applied voltage become important when the resistance of the junction becomes comparable to the finite input resistance (20 kilohms) of our electrometer.
12. To determine tip-surface separation, we have compared the measured *I* versus *D* curves for the "bare" tips to a calculation by Lang (*13*), which models the STM junction as two jellium surfaces with a single atom adsorbed on one of the surfaces. This calculation shows that an impedance of 2×10^7 ohms for an STM junction corresponds to a tip height above the surface of ~7 Å. We have found Lang's calculation to be consistent with *I* versus *D* measurements taken on this same Ni surface (*6*). We used this calibration, together with the measured changes in tip height due to the presence of one or two Xe atoms in the junction, to determine the tip-surface separation.
13. N. D. Lang, *Phys. Rev. Lett.* **36**, 8173 (1987); J. K. Gimzewski and R. Möller, *Phys. Rev. B* **36**, 1284 (1987).
14. V. Kalmeyer and R. B. Laughlin, *Phys. Rev. B* **35**, 9805 (1987).
15. N. D. Lang, *Solid State Phys.* **28**, 225 (1973).
16. D. R. Hamann, M. Schlüter, C. Chiang, *Phys. Rev. Lett.* **43**, 1494 (1979); G. B. Bachelet, D. R. Hamann, M. Schlüter, *Phys. Rev. B* **26**, 4199 (1982).
17. We set $d = 2.6$ Å, the equilibrium Xe binding distance (*18*), except when $s < 2.6$ Å where we then set $s = d$ to account for the compression of the Xe atom.
18. N. D. Lang, *Phys. Rev. Lett.* **46**, 842 (1981).
19. See, for example, R. Landauer, *Phys. Scr.* **T42**, 110 (1992); *J. Phys. Condens. Matter* **1**, 8099 (1989); Y. Imry, in *Directions in Condensed Matter Physics: Memorial Volume in Honor of Shang-keng Ma*, G. Grinstein and G. Mazenko, Eds. (World Scientific, Singapore, 1986), pp. 101–163.
20. M. Büttiker, *IBM J. Res. Dev.* **32**, 63 (1988); E. O. Kane, in *Tunneling Phenomena in Solids*, E. Burstein and S. Lundqvist, Eds. (Plenum, New York, 1969), pp. 1–11.
21. C. Joachim *et al.*, *Europhys. Lett.* **20**, 697 (1992).
22. We thank D. J. Auerbach, R. Landauer, C. P. Lutz, and C. T. Rettner for helpful discussions. We are also indebted to C. P. Lutz for technical assistance.

12 February 1996; accepted 29 April 1996

Shape-Controlled Synthesis of Colloidal Platinum Nanoparticles

Temer S. Ahmadi, Zhong L. Wang, Travis C. Green, Arnim Henglein, Mostafa A. El-Sayed*

The shapes and sizes of platinum nanoparticles were controlled by changes in the ratio of the concentration of the capping polymer material to the concentration of the platinum cations used in the reductive synthesis of colloidal particles in solution at room temperature. Tetrahedral, cubic, irregular-prismatic, icosahedral, and cubo-octahedral particle shapes were observed, whose distribution was dependent on the concentration ratio of the capping polymer material to the platinum cation. Controlling the shape of platinum nanoparticles is potentially important in the field of catalysis.

Colloidal metal particles are of interest because of their use as catalysts (*1*), photocatalysts (*2*), adsorbents and sensors (*3*), and ferrofluids (*4*) and because of their applications in optical (*5*), electronic (*5*), and magnetic devices (*3*). Catalytic reactivity depends on the size and the shape of the nanoparticles, and therefore the synthesis of well-controlled shapes and sizes of colloidal particles could be critical for these applications.

Many studies on colloidal particles have focused on the control of particle sizes and their growth kinetics and have related particle size and catalytic activity (*6*). Moreover, research has shown that the degree of polymerization (*1*) and the concentration of the stabilizing polymer (*2*, *7*) influence the size distribution, stability, and catalytic activity of colloidal particles. For example, a recent study (*7*) has shown that a higher ratio of capping material to metal produces smaller Au particles. However, shape control has been much more difficult to achieve, and the influence of particle shape on catalytic activity has not been reported to date.

The morphology of colloidal Au has been studied (*8*, *9*), and shape-controlled synthesis of Au particles forming platelike trigons has been explained (*10*) in terms of the Kossel-Stranski theory of face-selective growth of crystals. Shape-controlled synthesis of polymer-protected Cu particles exhibiting platelike hexagonal morphology has also been reported (*11*). Recently, the morphologies of Pt colloidal particles were studied by means of ultraviolet-visible spectrophotometry and transmission electron microscopy (TEM) (*12*). A parameter *S*, derived from the optical spectrum, has been suggested as a measure of particulate shape and the degree of dispersion (*12*).

In this report, we describe a method for the synthesis of colloidal Pt nanoparticles with controlled shapes. By changing the ratio of the concentration of the capping material to that of Pt^{2+} at room temperature, we were able to change the distribution of Pt nanoparticle shapes.

The Pt nanoparticles were prepared by the method of Rampino and Nord (*13*) and Henglein *et al.* (*14*). A solution of 1×10^{-4} M K_2PtCl_4 was prepared in 250 ml of water, to which we added 0.2 ml of 0.1 M sodium polyacrylate (sample 1). We then bubbled Ar gas through the solution for 20 min. We then reduced the Pt ions by bubbling H_2 gas at a high flow rate through the solution for 5 min. The reaction vessel was then sealed, and the solution was left overnight. After 12 hours, the solution turned lightly golden and the absorption spectrum showed the formation of colloidal Pt. We prepared samples 2 and 3 by adding to the starting solution 1.0 and 0.5 ml of the 0.1 M polyacrylate solution, respectively, and following the same procedure. The initial ratios of the concentration of the capping material to that of the metal cation in the solution were therefore 1:1, 5:1, and 2.5:1 in samples 1, 2, and 3, respectively.

Because the concentration of the capping polymer was changed in the preparation of samples 1 through 3, the pH values of the starting solutions were also different. The variation of pH in the three solutions was small; it changed from 7.5 to 7.65 when the concentration of the polymer was changed by a factor of 5 (going from sample 1 to sample 2). In our synthesis, we adjusted the initial pH of the solutions to 7.5 in all three solutions.

We investigated the structures of the Pt particles using a Hitachi HF-2000 field emission gun TEM (200 kV) with a point-to-point image resolution of better than 0.23 nm and a lattice resolution of 0.1 nm. We recorded the experimental images digitally using a charge-coupled device camera, which allows subsequent processing and quantitative modeling. We prepared the

T. S. Ahmadi, T. C. Green, M. A. El-Sayed, School of Chemistry and Biochemistry, Georgia Institute of Technology, Atlanta, GA 30332, USA.
Z. L. Wang, School of Material Sciences and Engineering, Georgia Institute of Technology, Atlanta, GA 30332, USA.
A. Henglein, Hahn-Meitner Institut, Abteilung Kleinteilchenforschung, 14109 Berlin, Germany.
*To whom correspondence should be addressed.

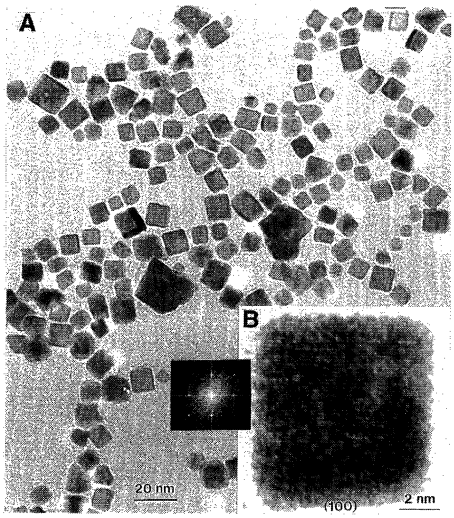

Fig. 1. (**A**) Low-magnification TEM image of sample 1, showing the size and shape distribution of the cubic particles. (**B**) High-resolution lattice image of a cubic Pt oriented with [100] parallel to the incident beam; the Fourier transform of the lattice image gives the optical diffractogram of the particle (inset), which explicitly shows the presence of the {100} facet.

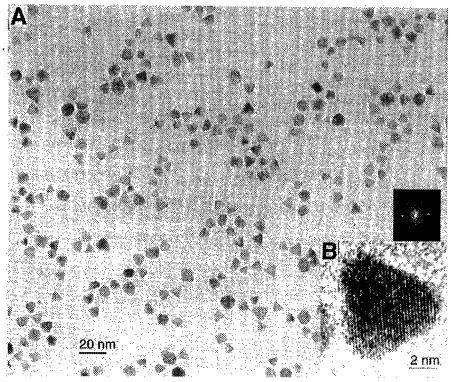

Fig. 2. (**A**) Low-magnification TEM image of sample 2, indicating the abundance of tetrahedra. (**B**) High-resolution image of a tetrahedral particle; the Fourier transform of the lattice image gives the optical diffractogram of the particle (inset). These particles are different from the rounded-corner triangular platelets observed in Au and Ag (*16*).

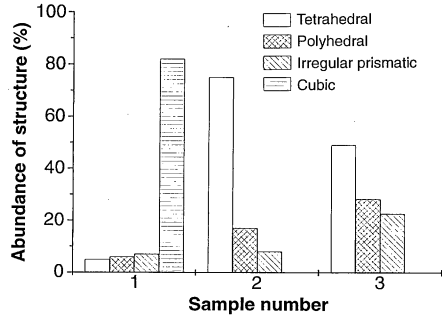

Fig. 3. Histogram showing the abundance of different shapes within each sample. Cubes are predominant in sample 1 and tetrahedra are predominant in sample 2. The shape abundances were measured from enlarged TEM images; we measured about 450 particles for each sample.

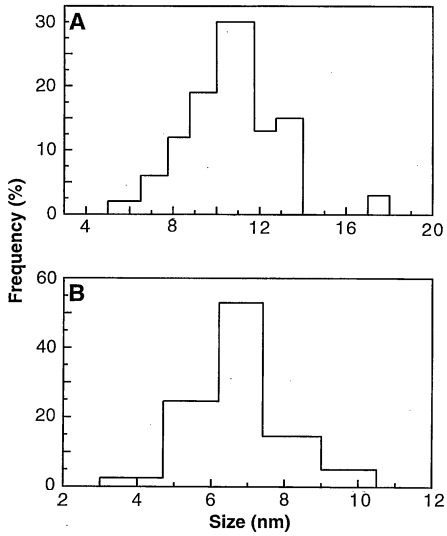

Fig. 4. (**A**) Size distribution of cubic particles formed in sample 1. (**B**) Size distribution of tetrahedra in sample 2. We obtained the size distributions from enlarged TEM images by counting 400 particles from each sample. Three trials for each sample were performed (a total of 1200 counts).

TEM specimens by dispersing Pt particles on amorphous C films that were less than 20 nm thick.

Sample 1 predominately contained particles with a square outline (Fig. 1), whereas samples 2 and 3 contained high proportions of particles with a triangular outline (Fig. 2). By tilting the samples in the TEM, we were able to determine the three-dimensional shapes of the particles. The particles with square outlines were found to be cubic, and those with triangular outlines were tetrahedral.

We measured the shape and size distributions of the particles from enlarged photographs of the TEM images (Fig. 3). Sample 1 contained 80% cubic particles, and sample 2 was dominated by tetrahedra with some small percentages of polyhedra and irregular-prismatic particles. These shapes have previously been observed in Pt colloids (*14*). Sample 3 contained a mixture of tetrahedra, polyhedra, and irregular-prismatic particles.

The formation of tetrahedral and cubic particles in samples 1, 2, and 3 has been reproduced three times. In each preparation of sample 2, about 60 ± 10% of the relative population of particles had tetrahedral shapes. The formation of cubic particles in sample 1 was reproducible to within 60 ± 20%. Whenever the concentration of cubic particles in sample 1 decreased, the concentration of other identifiable shapes also decreased, but the concentration of shapeless particles increased.

We measured the size distribution of each shape of the particles formed in each sample from the enlarged TEM images. For cubes and tetrahedra, the longest side of the two-dimensional images was used in the size distribution, whereas for polyhedra the longest diameters were considered. In sample 1, the cubic structure was dominant and other structures were minor. The average size of the cubic particles in sample 1 was 11.0 ± 0.5 nm (Fig. 4A), with sizes ranging from 4 to 18 nm. The size distribution of tetrahedra formed in sample 2 ranged from 4 to 10 nm, with an average size of 7.0 ± 0.5 nm (Fig. 4B). Sample 3 showed a similar size distribution, with an average size of 8.0 ± 0.5 nm. The difference in the average sizes between samples 2 and 3 is within the error range of the measurements. Similar average particle sizes (8.0 nm) were found for the polyhedra in samples 2 and 3, although the size distribution was wider in sample 3 than in sample 2. On average, smaller particles of irregular-prismatic structure were formed in sample 2 than in sample 3. In the latter, a wider distribution of irregular-prismatics was formed.

Our results demonstrate that using the same capping material, the same salt, the same temperature, and the same solvent but changing the ratio of the concentration of the capping material (sodium polyacrylate) to that of Pt ions produces different shapes of Pt nanoparticles. Cubes and tetrahedra are probably different expressions of the same type of nuclei, that is, face-centered-cubic. What determines the final shapes of these particles is the relative growth rate on {100} and {111}.

The mechanism of shape- or morphology-dependent synthesis of colloidal nanoparticles is not yet known. To determine the factors responsible for the control of the shape of Pt nanoparticles, a detailed study of the dependence of the shape distribution on such solution properties as pH, ionic strength, viscosity, and temperature will need to be done (*15*).

REFERENCES AND NOTES

1. H. Hirai, H. Wakabayashi, M. Komiyama, *Chem. Lett.* **1983**, 1047 (1983).
2. P.-A. Brugger, P. Cuendet, M. Gratzel, *J. Am. Chem. Soc.* **103**, 2923 (1981).
3. J. M. Thomas, *Pure Appl. Chem.* **60**, 1517 (1988).
4. S. C. Charles and J. Popplewell, in *Ferromagnetic Materials*, E. P. Wohlharth, Ed. (North-Holland, Amsterdam, 1980), vol. 2.
5. G. Schon and U. Simon, *Colloid Polym. Sci.* **273**, 202 (1995).
6. J. H. Clint *et al.*, *Faraday Discuss. Chem. Soc.* **95**, 219 (1993).
7. D. V. Leff, P. C. Ohara, J. R. Heath, W. M. Gelbart, *J. Phys. Chem.* **99**, 7036 (1995).
8. J. Turkevich, P. C. Stevenson, J. Hillier, *J. Discuss. Faraday Soc.* **11**, 55 (1951).

9. W. O. Milligan and R. H. Morriss, *J. Am. Chem. Soc.* **86**, 3461 (1964).
10. B. Bruche, *Kolloid-Z.* **170**, 97 (1960).
11. A. C. Curtis *et al.*, *Angew. Chem. Int. Ed. Engl.* **27**, 1530 (1988).
12. D. G. Duff, P. P. Edwards, B. F. G. Johnson, *J. Phys. Chem.* **99**, 15934 (1995).
13. L. D. Rampino and F. F. Nord, *J. Am. Chem. Soc.* **63**, 2745 (1942).
14. A. Henglein, B. G. Ershov, M. Marlow, *J. Phys. Chem.* **99**, 14129 (1995).
15. T. S. Ahmadi *et al.*, in preparation.
16. A. I. Kirkland, P. P. Edwards, D. A. Jefferson, D. G. Duff, *Annu. Rep. Prog. Chem. Sect. C* **87**, 247 (1990).
17. We thank the Office of Naval Research (grant N00014-95-1-0306) for its financial support of this project.

12 December 1995; accepted 25 April 1996

A Benzene-Thermal Synthetic Route to Nanocrystalline GaN

Yi Xie, Yitai Qian,* Wenzhong Wang, Shuyuan Zhang, Yuheng Zhang

A thermal reaction of Li_3N and $GaCl_3$ in which benzene was used as the solvent under pressure has been carried out for the preparation of 30-nanometer particles of gallium nitride (GaN) at 280°C. This temperature is much lower than that of traditional methods, and the yield of GaN reached 80%. The x-ray powder diffraction pattern indicated that sample was mainly hexagonal-phase GaN with a small fraction of rocksalt-phase GaN, which has a lattice constant a = 4.100 angstroms. This rocksalt structure, which had been observed previously only under high pressure (at least 37 gigapascals) was observed directly with high-resolution electron microscopy.

Hexagonal GaN with the wurtzite structure is a direct band-gap semiconductor with wide band gap (3.39 eV at room temperature) (*1*). It has potential applications in light-emitting devices in the visible to ultraviolet region (*2*). GaN with the rocksalt structure has been detected previously with energy-dispersive x-ray-diffraction for samples prepared in diamond-anvils. The phase that forms at ultrahigh pressure (≥37 GPa) disappeared as the pressure was released (*3*).

Johnson *et al.* (*4*) first prepared hexagonal GaN through the following reaction at temperatures above 900°C:

$$2Ga + 2NH_3 \rightarrow 2GaN + 3H_2$$

Usually, powder samples of hexagonal GaN were synthesized by placing some source materials such as $GaCl_3$ or $Ga(CH_3)_3$ under flowing ammonia at temperatures from 600° to 1000°C (*5*). Recently, precursors such as $[H_2GaNH_2]_3$ or $Ga(C_2H_5)_3NH_3$, which already have a Ga–N bond, could be pyrolysized to produce GaN at relatively low temperatures, but posttreatment temperatures >500°C are needed (*6*).

Nitrides of lanthanide and transition metals (M) can be synthesized through solid-state metathesis reactions such as:

$$MCl_n + Li_3N \rightarrow MN + LiCl$$

in the temperature range from 600 to 1100°C (*7*). However, the reaction of $GaCl_3$ with Li_3N through a similar process for the preparation of GaN failed (*8*).

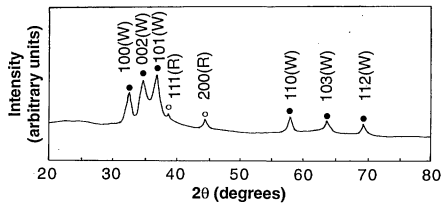

Fig. 1. An XRD pattern of nanocrystalline GaN.

We report on the reaction of Li_3N with $GaCl_3$ in benzene at 280°C under pressure in an autoclave. Nanocrystalline GaN was produced through what may be a liquid-solid reaction:

$$GaCl_3 + Li_3N \xrightarrow{\text{benzene}} GaN + 3LiCl$$

We call this technique a benzene thermal process, which is similar to a hydrothermal process, except that benzene is substituted for water.

In order to ensure the quality of the chemical reagent, Li_3N (*9*) and anhydrous $GaCl_3$ (*10*) were synthesized according to previously reported methods.

An appropriate amount of $GaCl_3$ solution in benzene and Li_3N powder was put into a silver-liner stainless steel autoclave of 50-ml capacity, and then the autoclave was filled with benzene up to 75% of the total volume. The air dissolved in the solution was driven off by passing argon gas through the solution. The autoclave was maintained at 280°C for 6 to 12 hours and then allowed to cool to room temperature. A dark-gray precipitate was collected that was washed with absolute ethanol to remove LiCl. The final product was dried in vacuum at 100°C for 2 hours.

The x-ray powder diffraction (XRD) pattern was recorded on a Japan Rigaku Dmax γA x-ray diffractometer with CuKα radiation (λ = 1.54178 Å). In the XRD pattern (Fig. 1), reflections marked with dots can be indexed to the hexagonal cell of GaN with lattice constants a = 3.188 Å and c = 5.176 Å, which are near the reported values (*11*). However, an unusually strong (002) peak in the pattern indicates a preferential orientation of [001] in nanocrystalline GaN. Other small reflections (marked with circles) can be indexed to cubic GaN in rocksalt structure with a = 4.100 Å, which is greater than the reported value of 4.006 Å at 50 GPa (*3*). The curve of volume versus pressure (*3*) shows that the

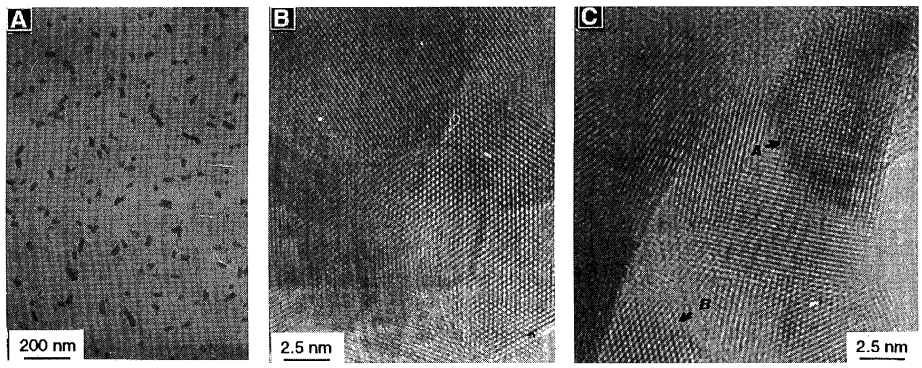

Fig. 2. (**A**) A TEM micrograph of nanocrystalline GaN. (**B** and **C**) HREM images of nanocrystalline GaN: (B) Lattice fringes of (001) plane in GaN with a wurtzite structure and (C) lattice fringes of (100) and (110) planes in GaN (marked A and B, respectively) with a rocksalt structure.

Y. Xie and Y. Qian, Structure Research Laboratory and Department of Applied Chemistry, University of Science and Technology of China, Hefei, Anhui 230026, People's Republic of China.
W. Wang, Department of Applied Chemistry, University of Science and Technology of China, Hefei, Anhui 230026, People's Republic of China.
S. Zhang and Y. Zhang, Structure Research Laboratory, University of Science and Technology of China, Hefei, Anhui 230026, People's Republic of China.
*To whom correspondence should be addressed.